AXON VOLTAGE-CLAMP SIMULATIONS

III. POSTSYNAPTIC REGION

RONALD W. JOYNER, JOHN W. MOORE, *and* FIDEL RAMÓN

From the Department of Physiology and Pharmacology, Duke University Medical Center, Durham, North Carolina 27710

ABSTRACT This is the third in a series of four papers in which we present the numerical simulations of the application of the voltage clamp technique to excitable cells. In this paper we discuss the problem of voltage clamping a region of a cylindrical cell using microelectrodes for current injection and voltage recording. A recently developed technique (Llinás et al., 1974) of internal application of oil drops to electrically insulate a short length of the postsynaptic region of the squid giant synapse is evaluated by simulation of the voltage clamp of an excitable cylindrical cell of finite length with variable placement of the current and voltage electrodes. Our results show that E_{Na} can be determined quite accurately with feasible oil gap lengths but that the determination of the reversal potential for the synaptic conductance, E_s, can be considerably in error. The error in the determination of E_s depends on the position of the microelectrode, the length of the oil gap, and especially the membrane resistance at the time the synaptic conductance occurs. It is shown that the application of tetraethylammonium chloride to block the active potassium conductance very significantly reduces the error in the determination of E_s. In addition we discuss the effects of cable length and electrode position on the apparent amplitude and time course of the synaptic conductance change. These results are particularly relevant to the application of the voltage clamp technique to cells with nonsomatic synapses. The method of simulation presented here provides a tool for evaluation of voltage clamp analysis of synaptic transmission for any cell with known membrane parameters and geometry.

INTRODUCTION

The quality of our understanding of some properties of synaptic transmission has become dependent upon the quality of the voltage control of the postsynaptic regions. Therefore it is important to evaluate how well such an attempt can succeed and that is the purpose of this paper.

The first two papers in this group (Moore et al., 1975 *a, b*) have presented a method for numerical solution of the membrane potential and current distribution of a cylindrical cell (axon) in the feedback loop of a simulated voltage clamp circuit. The axon is simulated as an active cable in which each membrane segment is endowed with the ionic conductances as described by Hodgkin and Huxley (1952) equations for the squid giant axon.

In this paper we add the complexity of a conductance change in a synaptic region

as the result of transmitter release from a presynaptic terminal as a result of the arrival of an impulse. Space clamp conditions are technically difficult to achieve at the synaptic regions of many kinds of cells. Usually access to the interior of the synaptic region is via microelectrodes, one to inject current and one to measure the potential.

Several attempts have been made to determine the potential at which synaptic currents in the squid giant synapse reverse and the reported values range from ϕ mV (Hagiwara and Tasaki, 1958) to +45 mV (Gage and Moore, 1969). It seems possible that part of the differences may reflect different qualities of space clamp conditions. In the second paper of this series (Moore et al., 1975 *b*) it was shown that the segment in which the voltage is sensed was the only one which was actually "clamped" in an axon in which the axial resistance is not shunted by a wire. Thus it was important to know the actual voltage profile along the axon for several experimental situations and conditions.

Attempts to "voltage clamp" a postsynaptic region of axon by injection of current at a point or over a short length are certainly subject to error, especially as the membrane is strongly depolarized. One purpose was to see just how bad such voltage errors had been and how much they affected the measurement of the reversal potential. It was clear that if the postsynaptic region was short and if it could be electrically isolated from the rest of the axon, much better voltage control should be possible and lead to better measurements of the reversal potential. Such isolation had been proposed[1] in the form of internal seals by replacement of axoplasm with oil drops. Therefore we also examined this case to study the feasibility of obtaining relatively good control of potential over the synaptic region. Our proposed experimental situation was simulated by having the control current injected at one point and the feedback voltage measured at another. This arrangement was diagrammed in Fig. 1 in the preceding paper.

In several previous reports (Hagiwara and Tasaki, 1958; Gage and Moore, 1969) the potential at which synaptic currents reversed had been measured and compared with published values of E_{Na}, the sodium equilibrium potential. Because it is known that E_{Na} changes with time and axon deterioration (Moore and Adelman, 1961) it seemed appropriate to attempt to measure and compare both potentials in the same experiment and at the same time. Therefore in our simulations we examined whether one could in fact measure the actual sodium equilibrium potential without errors introduced by the voltage inhomogeniety. Additional simulations investigated the correspondence between the actual and apparent reversal potentials for synaptic currents. Part of the object of these studies was to see if there might be any reconciliation of the reported values for the reversal potential by applying corrections developed as a result of the simulations.

Most of the emphasis in these simulations was placed on the evaluation of the quality of the proposed oil-drop isolation experiment. The simulations indicated that, although the quality of the voltage clamp was marginal, it was feasible. Furthermore the simulations provided ways to correct for errors in measurement arising from the

[1] Llinas, R., R. W. Joyner, and C. Nicholson. 1975. *J. Gen. Physiol.* In press.

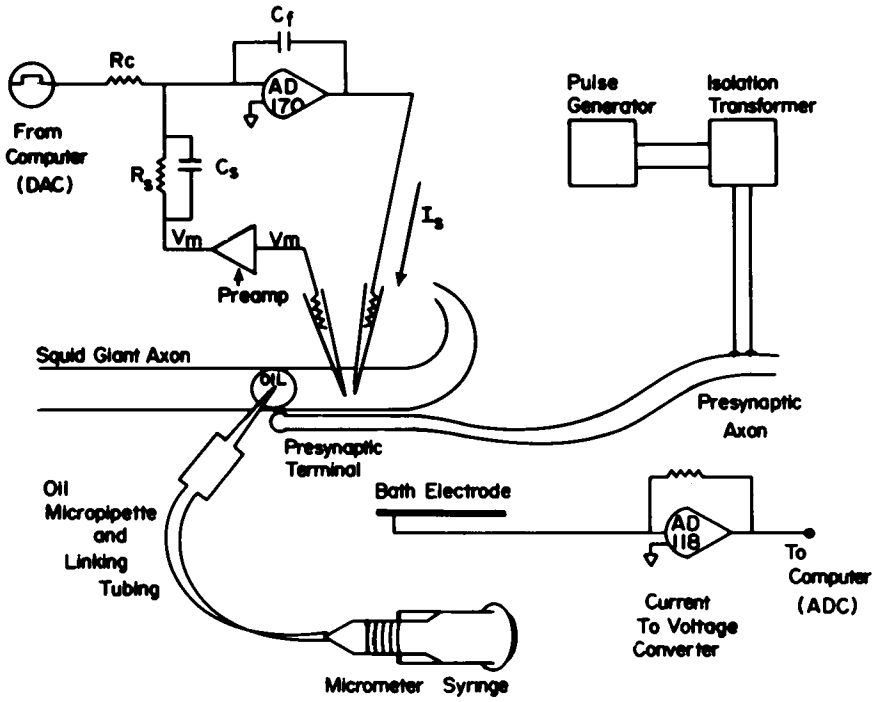

FIGURE 1 Schematic diagram of the experimental arrangement; oil is injected by pressure from the micrometer syringe. The voltage clamp circuit with the current and voltage electrodes in the synaptic region is also shown.

lack of voltage homogeneity. Therefore the proposed experiments were carried out. Electrical insulation of the postsynaptic region of the squid giant synapse from the rest of the giant axon was accomplished by pressure injection of paraffin oil inside the axon and the experimental results are described elsewhere.[1] The basic scheme is illustrated in Fig. 1. The presynaptic terminal is 30–50 μm in diameter and makes synaptic contact for a length of about 1 mm on a postsynaptic axon of 100–200 μm diameter. Microelectrodes were used to measure the membrane potential and to inject the current from the voltage clamp circuit.

METHODS

The method for solution of the active cable equations and the voltage clamp circuit equations has been described in the earlier papers (Moore et al., 1975 *a,b*) except that here we will use the standard H-H values for $\bar{g}_{NA}$ and $\bar{g}_K$. The only modification to the equations required to include synaptic transmission is to add (to selected cable segments) a variable synaptic conductance in series with an electromagnetic force corresponding to the reversal potential for the synaptic current. The variable synaptic conductance was modeled either as a step (pulse) conductance change or as a modified exponential function to generate a transient change with a fast rise and slower decline.

RESULTS

Voltage Clamp

When a passive cable is voltage "clamped" by injecting current at one segment and recording potential from one segment, both the transient and steady-state potentials are nonuniform along the cable. Fig. 2 illustrates the time course of voltage changes in a five-segment passive cable with each segment having specific membrane resistance 1,000 Ω-cm^2, length 100 μm, and diameter 200 μm. Both the current and voltage electrodes are in the central segment. The voltage at segments 1, 2, and 3 are shown as functions of time (by symmetry, segments 4 and 5 correspond to segments 2 and 1, respectively). The potential at the central segment rises quickly to the control potential (100 mV); but, as the distance from the central segment increases, the potential rises more slowly and reaches a lower value in the steady state.

A similar but more complicated voltage and current deviation along the cable occurs if the cable is now endowed with excitable (Hodgkin-Huxley, 1952) membrane properties. When the excitable membrane is depolarized, the sodium conductance rapidly increases, tending to drive the membrane potential toward the sodium equilibrium potential of +115 mV (with respect to the resting potential) and then the potassium conductance increases, tending to drive the membrane potential in the opposite direction (toward the potassium equilibrium potential of −12 mV). Fig. 3 shows the results of such a simulation for a point clamp of a 200 μm diameter axon. In each case the voltage and current electrodes are placed in the central segment of a five-segment cable, but the length of the cable is 500, 1,000, and 2,000 μm in Fig. 3 A, B, and C, respectively. The membrane potential and membrane current densities of the central segment and a terminal segment are plotted, along with the total membrane current density. In Fig. 3 A the cable is short and nearly isopotential such that the membrane potential and current distributions are approximately uniform at all times. In Fig. 3 B and C, when the cable is made successively longer, it is clear that only the central segment is actually clamped, while the others show the expected positive and negative

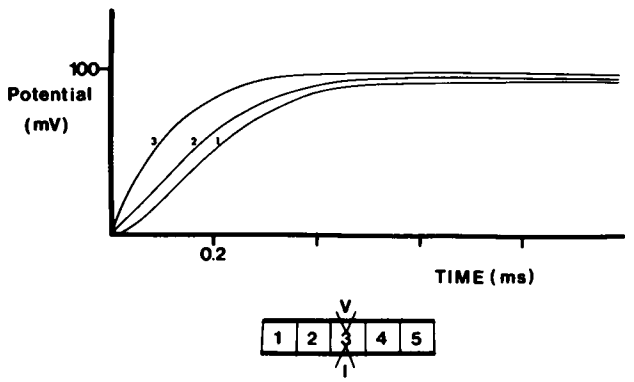

FIGURE 2 Voltage response at three segments for the voltage control at the central segment of the cable shown; each segment is 100 μm and the diameter is 200 μm.

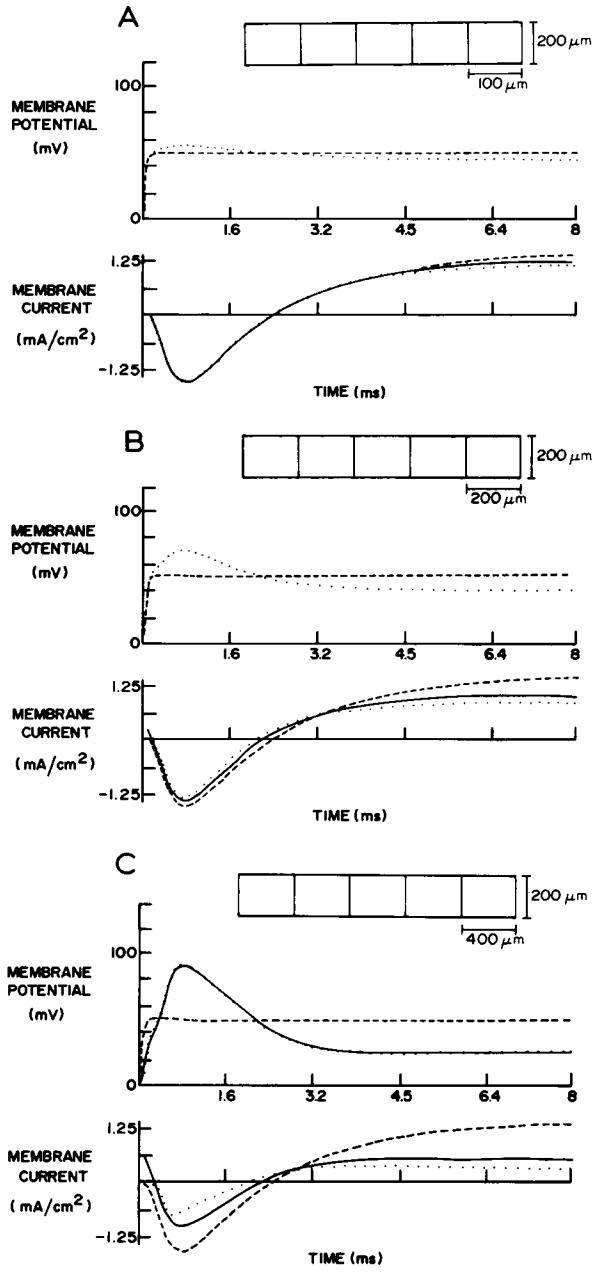

FIGURE 3 Plots of the membrane potentials, membrane current densities, and the normalized sum of the membrane currents for the voltage control of the three active cables shown in the inserts. In each case the depolarizing pulse potential is 50 mV. In each plot the dots and dashes correspond to the terminal and central segments, respectively, while the solid line in the current plot is the normalized sum of the membrane currents (corresponding to what would be experimentally measured).

voltage deviations from the control potential. These deviations increase with distance from the control point. The membrane currents at each segment are different, and the measured sum of the currents corresponds neither in amplitude nor in time course to the current of any of the individual segments. As the distance from the control point increases, both the initial sodium and the later potassium currents are reduced. It is clear from Fig. 3 C that even if some parts of the cable are essentially uncontrolled, giving partial action potentials, the measured sum of the currents still appears to resemble the shape reported for an isopotential patch of membrane. However, it is obvious that this current does *not* accurately reflect the membrane current of any segment of the cable. This result is not only consistent with the previous analysis of a point clamp by a simplified "two patch" model (Taylor et al., 1960) but also provides a quantitative evaluation of the system.

Determination of Sodium Equilibrium Potential

Another important problem is the effect of the cable properties on the determination of the sodium equilibrium potential, E_{Na}. It may well be that the voltage nonuniformities shown above may cause serious errors in the determination of E_{Na}. To our knowledge, this system has not been studied even with an over-simplified model. This problem is readily examined by using the simulations as described above and plotting the peak of the early current against the control potential.

There are two factors which may make determination of E_{Na} from experimental records difficult. At the high depolarizations needed to reverse the sodium current, the leakage current is large and the potassium current turns on quickly, masking the sodium current. Furthermore, if the voltage clamp is slow, the sodium current may be obscured by the capacitive current. Hyperpolarization preceding the test pulse can improve the experimental determination of E_{Na} by increasing the sodium current resulting from a given voltage step and slowing the onset of potassium current (Cole and Moore, 1960). The determination of E_{Na} may be improved by the use of intracellular tetraethylammonium ions (TEA) (Armstrong and Binstock, 1965) to partially block the potassium conductance. This effect may be simulated by multiplying the maximum potassium conductance $\bar{g}_k$ by a scale factor, S_k, $(0 \leq S_k \leq 1)$. Fig. 4 shows the results of such a simulation, with S_k equal to 0.01 (an extremely low value) for an axon 100 μm in diameter and five segments each of 100 or 200 μm in length. The potential and current of the central segment and a terminal segment are plotted, along with the normalized sum of the currents for depolarizing potential steps of 80 and 135 mV (from the resting potential). For the short cable (500 μm, Fig. 4 A) the currents are nearly the same at each segment and correspond to the current sum except for the initial capacitative current, while in the longer cable (1,000 μm, Fig. 4 B) the individual segments show larger voltage and current deviations from the average.

In order to simulate the determination of the value of E_{Na}, the maximum values of the early membrane currents are plotted as functions of the control potential as shown in Fig. 5. The *I-V* curve for the short cable (1) has the correct slope and intercept for the sodium conductance. For the longer cable (2) the values of the early current are de-

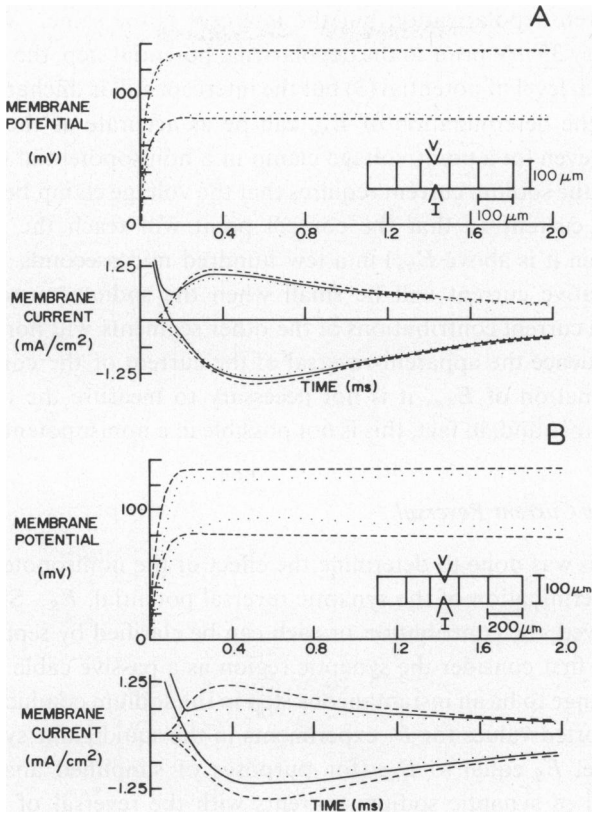

FIGURE 4 Plots of membrane potential and membrane current densities for depolarizing pulses of 80 and 135 mV with S_k = 0.01. The current density sum (solid line) and the potential and current densities for the central segment (dashes) and a terminal segment (dots) are shown for a five-segment active cable with the diameter and segment length as shown.

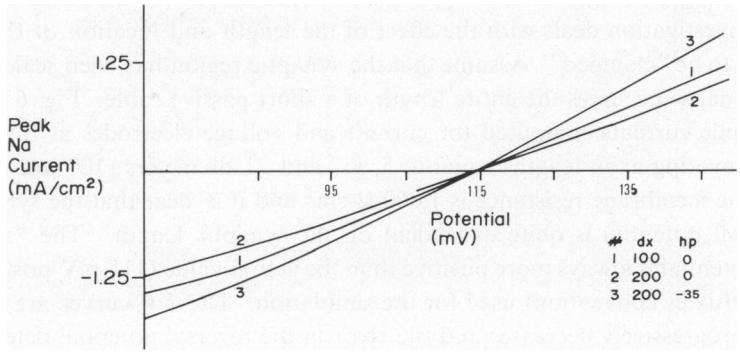

FIGURE 5 Plots of peak early currents vs. the control potential for the active cable of Fig. 4 A (1), Fig. 4 B (2), and the same cable as in Fig. 4 B but with a prior hyperpolarization of 35 mV (3).

creased for a given depolarization but the intercept is the same. When the cable is hyperpolarized by 35 mV prior to the depolarizing potential step, the early currents are increased for each level of potential (3) but the intercept still is unchanged.

In summary, the determination of E_{Na} can be as accurate as the measurement of sodium currents even for a point voltage clamp in a nonisopotential region. Accurate measurement of the sodium current requires that the voltage clamp be fast enough and provide enough current so that the control point will reach the desired potential (particularly when it is above E_{Na}) in a few hundred microseconds. This will insure that the capacitative current will be small when the sodium current occurs. The transient sodium current contributions of the other segments will normally occur later and will not influence the apparent reversal of the current of the controlled segment. For the determination of E_{Na}, it is not necessary to measure the true value of the sodium conductance and, in fact, this is not possible in a nonisopotential region.

Synaptic Current Reversal

A similar analysis was done to determine the effect of the nonisopotential cable properties on the determination of the synaptic reversal potential, E_S. Since a number of factors are involved, the contribution of each can be clarified by separation into components. Let us first consider the synaptic region as a passive cable and the synaptic conductance change to be an instantaneous step in the sodium conductance. Although some of the reported values for E_S experiments in the squid giant synapse have been lower, we will set E_S equal to E_{Na} (for purposes of simplified analysis), and compare the reversal of synaptic sodium currents with the reversal of Hodgkin-Huxley sodium current. We will continue to simulate the voltage clamp by having the feedback voltage coming from one specified segment and the control current being applied to another. The specific effects which we consider in sequence are: (*1*) the locations of the synaptic conductance change, (*2*) the placement of the voltage and current electrode, and (*3*) more realistic cable and synaptic descriptions.

In order to gain insight into the problem, we will start with a passive membrane. The first investigation deals with the effect of the length and location of the synapse in the area to be "clamped." Assume that the synaptic region has been sealed off such that the synapse occupies the entire length of a short passive cable. Fig. 6 shows the peak synaptic currents computed for current and voltage electrodes at the center of synapses covering axon lengths equal to 5, 11, and 21 diameters (100 μm diam). In Fig. 6 A the membrane resistance is 1,000 Ω-cm^2 and it is clear that the synaptic current reversal potential is quite dependent on the synaptic length. The "measured" reversal potential is always more positive than the actual value (115 mV positive in the Hodgkin-Huxley convention) used for the simulation. The *I-V* curves are linear but the slope progressively decreases and the error in the reversal potential determination increases. This effect is even more striking in an axon with a membrane resistance of 100 Ω-cm^2 which is close to the steady-state resistance in a depolarized axon (Fig. 6 B). In these simulations the area of synaptic contact was assumed to be the entire length

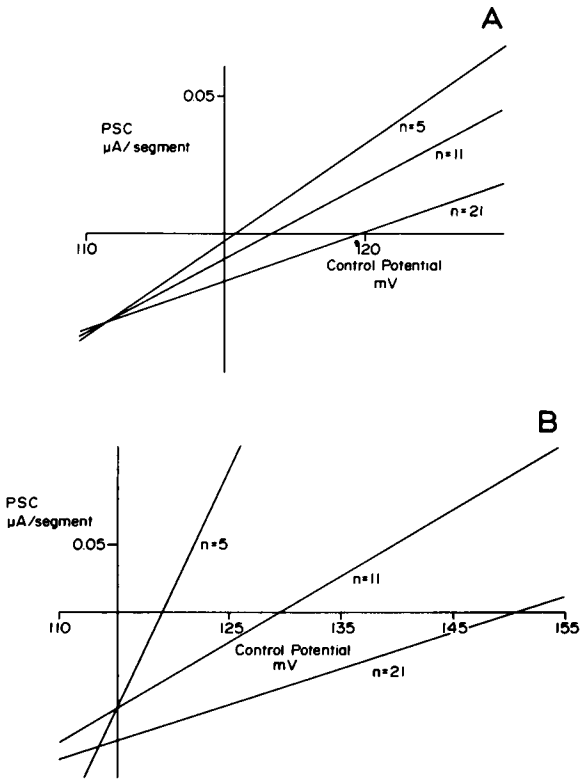

FIGURE 6 Plots of the peak synaptic current versus the control potential for passive cables with segment length and diameter equal to 100 μm. Synaptic transmission occurs along the entire length of the cable and the number of segments, n, is listed with each plot. The specific membrane resistance is 1,000 Ω-cm^2 for 6 A and 100 Ω-cm^2 for 6 B.

of a finite cable and both the current and voltage electrodes were assumed to be centrally placed. Therefore the error arose from the distributed nature of the synapse.

Different types of error occur when the synaptic contact is only a part of a long cable or the electrodes are not centrally placed with respect to the synaptic region. In each of these situations the voltage profile along the cable is no longer symmetrical with respect to the center point. In Fig. 7 the voltage gradients resulting from three different locations of the voltage and current electrodes are shown. In each case the segment at the voltage electrode is held at some voltage, V_c, by current supplied to the segment at the current electrode but the voltage profile is different for each configuration. In curve *B* the voltage for one-half of the cable is above V_c and the voltages at the other segments are below V_C, while in curves *A* and *C* all of the cable except the point being clamped is higher or lower, respectively, than V_c. Since the synaptic current at each segment is proportional to the difference between the reversal potential and the potential at that segment, it is clear that the apparent reversal potential measured with the electrode placement as in curve *A* will be lower than the true value and with the electrodes as in

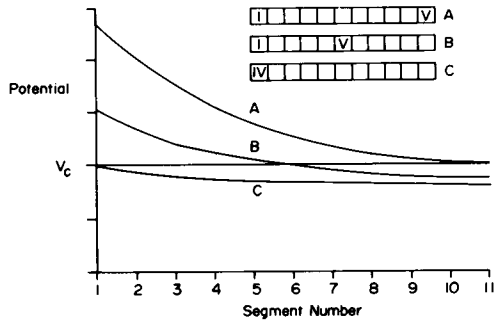

FIGURE 7 Voltage profiles along an eleven segment passive cable for a steady-state voltage clamp with three configurations of the current (I) and voltage (V) electrodes as shown. In each case, the segment with the voltage electrode is clamped to the control potential V_c.

curve C the apparent value will be higher than the true value, while the electrode positions as in curve B will give intermediate results.

To consider some of these effects quantitatively, simulations were done to determine the reversal potential for various placements of the voltage and current electrodes in cables still with passive membranes. The procedure was to voltage clamp the cable to some control potentials and then to turn on a synaptic conductance at selected segments and compute the difference in total membrane current before and after the synaptic conductance change. In Fig. 8 A, B, and C the percentage error in the determination of E_S is plotted against the segment number for the location of the electrode which is moved while in 8 D the percentage error is plotted against the number of segments. In each case the simulated cable is drawn to correspond with the horizontal axis of the plot and the voltage and current electrode positions are labeled.

In Fig. 8 A the synaptic conductance change occurs at all segments of an 11 segment cable. The voltage electrode is fixed in the central segment and the percentage error in E_S is shown as a function of the location of the current electrode. E_S is overestimated when both electrodes are in the central segment and underestimated when the current electrode is at either end (for which case the voltage profile is qualitatively that of curve B of Fig. 7). With the current electrode at segment 1, at each level of control potential, only the central segment is truly voltage clamped, and the positive deviations of the left half of the cable are greater than the negative deviations of the right half of the cable.

Fig. 8 B illustrates the results for the opposite extreme in which the current electrode is at the end of the cable and the voltage electrode is moved to different segments. The shift from positive to negative errors in the determination of E_S as the voltage electrode is moved away from the current electrode can be predicted from the qualitative potential profiles of curves B and C, Fig. 7. A similar set of plots may be generated by fixing the location of the voltage electrode and moving the current electrode.

Fig. 8 C shows the results of doubling the cable length by making each segment 200 instead of 100 μm long but including the synaptic conductance change at only the three

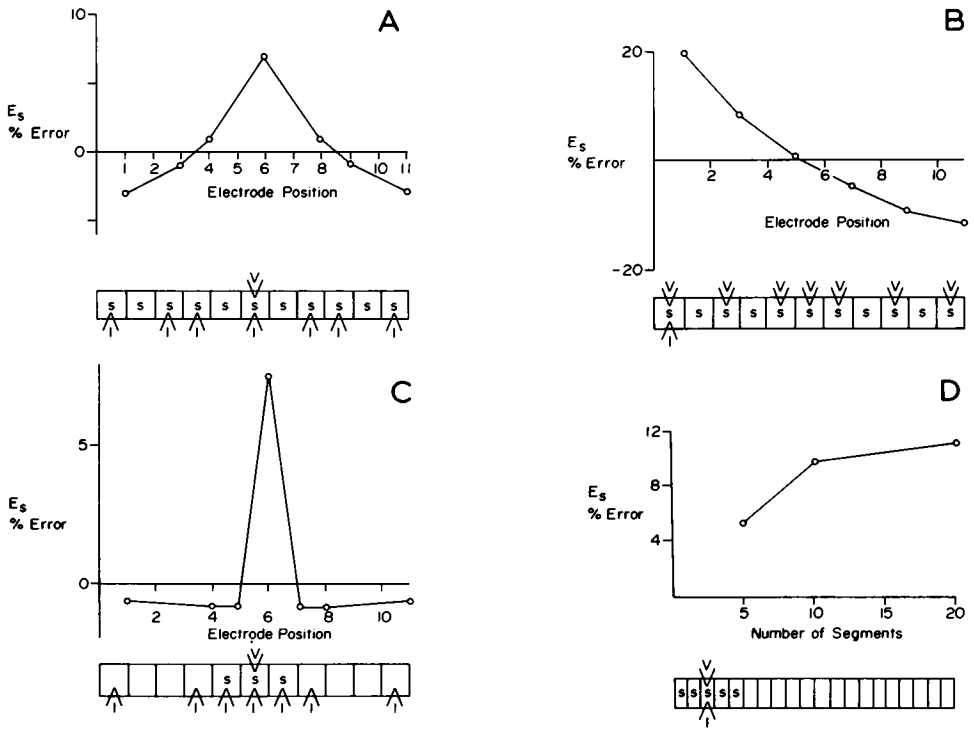

FIGURE 8 Percentage error in E_S as a function of electrode positions in 8 A, 8 B, and 8 C, and as a function of the number of segments in 8 D. In parts 8 A, 8 B, and 8 C one of the electrodes is fixed and the other is moved as shown. Segments with synaptic activity are labeled with "S." Specific membrane resistance is 100 Ω-cm^2, diameter is 200 μm, segment length is 100 μm for 8 A, 8 B, and 8 D and 200 μm for 8 C.

central segments. Since the error in the determination of E_S depends on the degree of isopotentiality within the synaptic region, the error is negative at the synaptic boundary as in Fig. 8 A but then does not continue to become more negative as the current electrode is moved toward the end of the cable but actually decreases.

Fig. 8 D shows the effect of adding on additional nonsynaptic segments to a five-segment cable with fixed current and voltage electrodes. The error increases due to the effect of the additional segments on the voltage profile in the synaptic region.

In summary, the simulations of the point clamp of passive cables have shown how errors in the reversal potential can arise from the distributed nature of the synapse, the placement of the electrodes, and the cable properties of the post synaptic region.

We will now introduce additional factors in order to make the simulations more realistic and comparable to the experimental situation. We will now (1) simulate a voltage clamp of a finite cable with a Hodgkin-Huxley membrane, and (2) replace the synaptic conductance step with a more realistic pattern. The synaptic conductance at the squid giant synapse reaches a peak in 0.5–1 ms and then declines with a time constant of about 1 ms. A simple function approximating this time course (for t in milli-

seconds) is:

$$g_s(t) = 4te^{-2t}. \tag{1}$$

For an active axon it is possible to make qualitative predictions about the error in the determination of E_S from the simulations of the reversal potential determination for passive cables. For centrally located electrodes, we observed that the error increases when the membrane resistance decreases, and that this error is always in a direction such that the apparent reversal potential is higher than the true E_S. When an active membrane is stepped to a depolarizing potential, there is a transient increase in the sodium conductance, then a slower rise in the potassium conductance to a steady value which depends on the membrane potential. Therefore, if synaptic transmission occurs during a nearly maximum steady-state potassium conductance, the membrane resistance is at a much lower value than in the resting state and, to a first approximation, could be considered as not too different from a passive cable with a low membrane resistance. However, since the potential profile along the cable depends on the membrane resistance and since the resistance at each segment depends on the potential it is necessary to do a complete simulation of the voltage clamp of an active cable to quantitatively appraise the expected errors. Because we are only interested in assessing the difference between the actual and apparent reversal potentials, we will continue the simulations with the actual reversal potential for the synaptic conductance, E_S, equal to E_{Na} (+115 mV).

The results of simulations of a short active cable with the synaptic conductance pattern given by Eq. 1 along the length of the cable are shown in Fig. 9. The potential

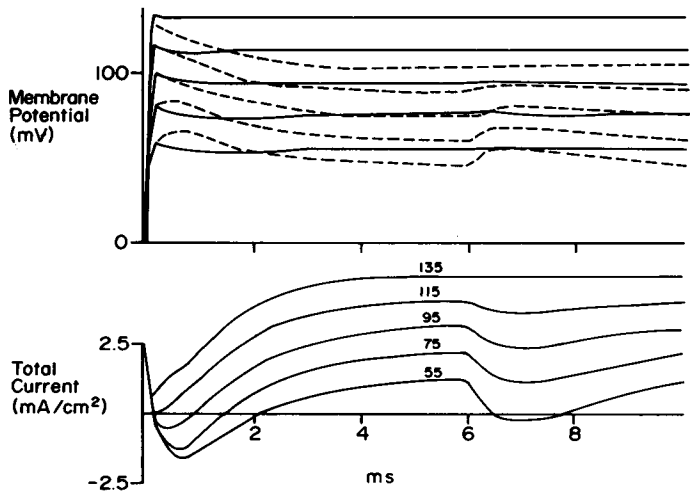

FIGURE 9 Plot of the membrane potential of the central segment (solid line) and a terminal segment (dashed line) for step clamps of 55, 75, 95, 115, and 135 mV along with the corresponding sum of the membrane current densities (lower part). The active cable has five segments of 200 μm each and a diameter of 200 μm. Synaptic transmission occurs at t = 6 ms, S_k = 1.0.

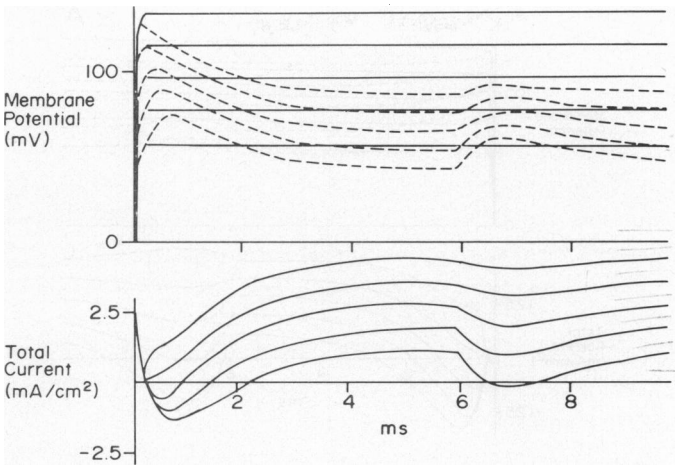

FIGURE 10 Plot of the membrane potential of the central segment (solid line) and a terminal segment (dashed line) for step clamps of 55, 75, 95, 115, and 135 mV along with the corresponding sum of the membrane current densities (lower part). The active cable has five segments of 200 μm each and a diameter of 100 μm. Synaptic transmission occurs at t = 6 ms. S_k = 1.0.

at the central segment and at the terminal segment are plotted as functions of time for control potentials of +55, +75, +95, +115, and +135 mV with respect to the resting potential. Note that for potentials below E_{Na} the potential of the central unit is well controlled while the terminal unit shows a transient positive deviation, then reaches a steady-state negative deviation, followed by a positive deviation when the synaptic conductance change occurs. The measured current is also shown below for the same command voltage steps. The active sodium current is inward at control potentials below E_{Na}, and outward for control potentials higher than E_{Na}.

In this simulation the normal Hodgkin-Huxley value for the potassium conductance was used (S_k = 1). The synaptic conductance change starts at 6 ms and it is clear that the synaptic current has not reversed in sign at the assigned E_S of +115 mV but is barely reversed in sign at a control potential of +135 mV, giving an error in the apparent E_S of about 20 mV. If the axon diameter is decreased from 200 to 100 μm, potential gradients are even larger and the apparent reversal potential is even higher (Fig. 10).

Going back to a 200 μm axon, we can simulate the effect of intracellular TEA on the determination of E_S. In Fig. 11 A, the potassium conductance is decreased to 40% of its normal value (S_k = 0.4) and the apparent synaptic reversal potential is about +125 mV; and, in Fig. 11 B where S_k = 0.05, the apparent reversal potential is very close to the assigned value of +115 mV.

If one could arrange a voltage clamp which could achieve the desired isopotentiality over the synaptic region, one could accurately measure not only the reversal potential for the synaptic conductance but also the amplitude and time course of the synaptic conductance. However when this is not the case serious errors can be made if one

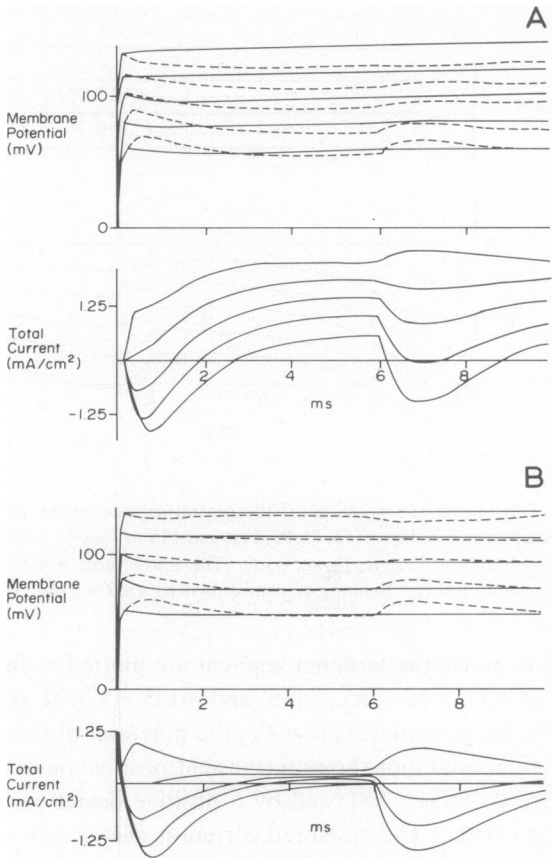

FIGURE 11 Plot of the membrane potential of the central segment (solid line) and a terminal segment (dashed line) for step clamps of 55, 75, 95, 115, and 135 mV along with the corresponding sum of the membrane current densities (lower part). The active cable has five segments of 200 μm each and a diameter of 200 μm. Synaptic transmission occurs at t = 6 ms. The TEA effect is simulated by letting S_k = 0.4 in 11 A and S_k = 0.05 in 11 B.

assumed it to be true. We will illustrate this with two arrangements. The first is one in which the synaptic region is a small part of a long cylindrical cell with the current and voltage electrodes within the synaptic region as is the case for the squid giant synapse or the neuromuscular junction. The second case is one in which the current and voltage electrode are together in a cell body but the synaptic region is separated from them by a region with cable properties; this corresponds to cells such as the spinal motoneurones in which many synapses occur on the dendrites.

These two configurations can be studied by simulating the voltage clamp of a long (11 segment) cable with both the current and voltage electrodes in the same (initial) segment. Fig. 12 shows simulations using a passive membrane resistance of 1,000 Ω-cm^2, a segment length of 400 μm, and a cable diameter of 50 μm. In each case, the upper graph shows the voltage at segments 1, 3, 5, 7, 9, and 11 while the lower graph

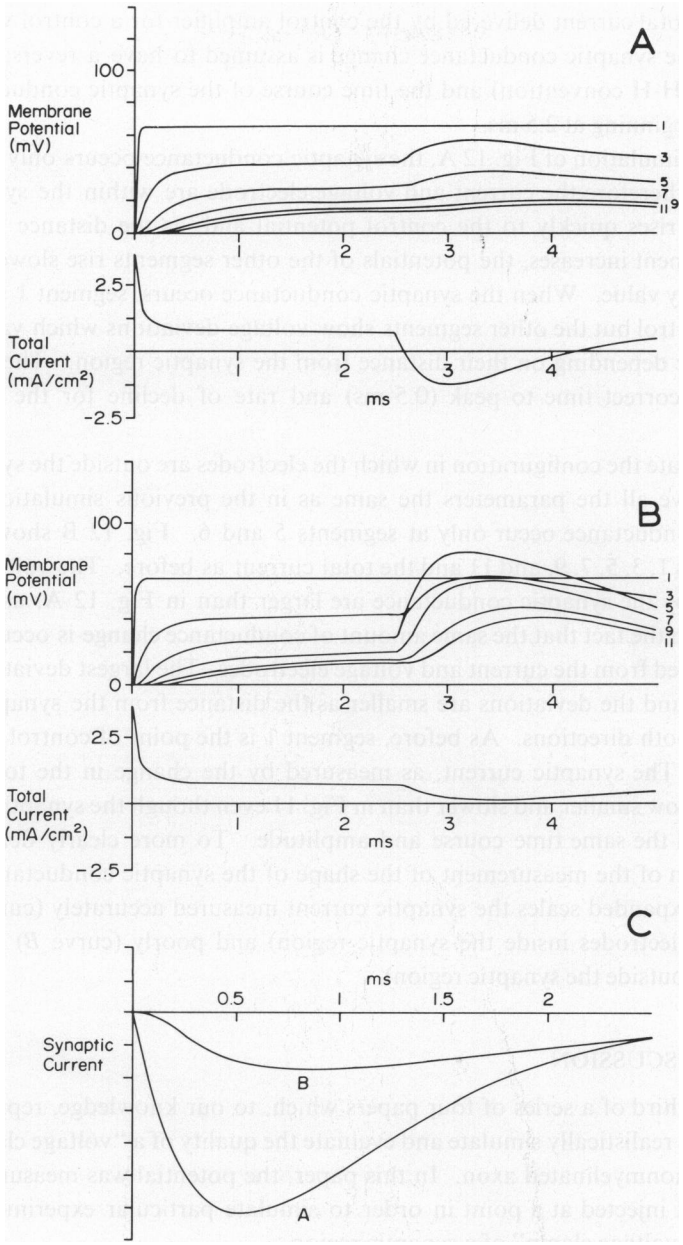

FIGURE 12 A Voltage at selected segments and total current density for the simulated voltage clamp of an 11-segment passive cable with the current and voltage electrode in segment 1. The synaptic conductance change occurs in segments 1 and 2, specific membrane resistance is 1,000 Ω-cm^2, diameter 50 μm, and segment length 400 μm.

FIGURE 12 B Voltage at selected segments and total current density for the simulated voltage clamp of an 11-segment passive cable with the current and voltage electrodes in segment 1. The synaptic conductance change occurs in segments 5 and 6, specific membrane resistance 100 Ω-cm^2, diameter 50 μm, and segment length 400 μm.

FIGURE 12 C Comparison of synaptic currents from the simulations of Fig. 12 A (curve *A*) and Fig. 12 B (curve *B*). The synaptic conductance had the same time course and amplitude for both simulations.

shows the total current delivered by the control amplifier for a control voltage step of 65 mV. The synaptic conductance change is assumed to have a reversal potential of +115 mV (H-H convention) and the time course of the synaptic conductance is given by Eq. 1, beginning at 2.5 ms.

For the simulation of Fig. 12 A, the synaptic conductance occurs only at segments 1 and 2 and therefore the current and voltage electrode are within the synaptic region. Segment 1 rises quickly to the control potential and, as the distance from the controlled segment increases, the potentials of the other segments rise slower and reach a lower steady value. When the synaptic conductance occurs, segment 1 remains under voltage control but the other segments show voltage deviations which vary in size and time course depending on their distance from the synaptic region. The current trace shows the correct time to peak (0.5 ms) and rate of decline for the synaptic conductance.

To simulate the configuration in which the electrodes are outside the synaptic region, we can leave all the parameters the same as in the previous simulation but let the synaptic conductance occur only at segments 5 and 6. Fig. 12 B shows the voltage at segments 1, 3, 5, 7, 9, and 11 and the total current as before. The voltage deviations produced by the synaptic conductance are larger than in Fig. 12 A, as might be expected from the fact that the same amount of conductance change is occurring at a site now removed from the current and voltage electrodes. The largest deviation occurs for segment 5 and the deviations are smaller as the distance from the synaptic region increases in both directions. As before, segment 1 is the point of control and shows no deviation. The synaptic current, as measured by the change in the total membrane current is now smaller and slower than in Fig. 11 even though the synaptic conductance change had the same time course and amplitude. To more clearly demonstrate this degradation of the measurement of the shape of the synaptic conductance, Fig. 12 C shows on expanded scales the synaptic current measured accurately (curve *A*) in 12 A (with the electrodes inside the synaptic region) and poorly (curve *B*) in 12 B (with electrodes outside the synaptic region).

DISCUSSION

This is the third of a series of four papers which, to our knowledge, represent the first attempts to realistically simulate and evaluate the quality of a "voltage clamp" of a segment of a nonmyelinated axon. In this paper, the potential was measured at a point and current injected at a point in order to simulate particular experimental arrangements for "voltage clamp" of a synaptic region.

The experimental determination of the sodium equilibrium potential has been made under a number of conditions in a variety of voltage clamp arrangements. It is most reassuring to learn from these simulations that the measurement is rather accurate even in the face of considerable nonuniformity in the voltage profile of a cable. For a nonisopotential voltage clamp, the measured active sodium currents are incorrect in amplitude and time course with respect to the amplitude and time course of the sodium con-

ductance at any of the segments, but they reverse in sign at the correct value of E_{Na}. We might also note here that we (Ramón et al., 1975) have shown (in our simulation of the double sucrose-gap voltage clamp of a bundle of nerve fibers) that the determination of E_{Na} is not disturbed by inclusion of a series resistance such that all regions of the bundle are uncontrolled.

It is instructive to compare the results for the determination of E_s with results for the determination of E_{Na}. The synaptic equilibrium potential is set equal to E_{Na}, so that only sodium ions are involved in the simulated synaptic current, yet the determination of E_S is seriously in error for nonisopotential regions. For the active sodium currents, the cable is quickly clamped to the control potential and the resting membrane conductance primarily determines the potential profile along the control potential and the resting membrane conductance primarily determines the potential profile along the cable before the active sodium conductance is turned on. However, in order to measure synaptic currents at various membrane potentials it is necessary to stimulate the presynaptic axon at a time such that the synaptic conductance change will occur after the potassium conductance has reached a steady-state value. This large conductance produces a much greater potential gradient at the time of the synaptic conductance than at the time of the Hodgkin-Huxley sodium conductance. In the passive cable simulations a specific resistance of 100 Ω-cm^2 was used to approximate this active condition. In addition, the active sodium conductance at each segment is a function of the voltage at the segment as opposed to the synaptic conductance which is assumed not to be voltage dependent. Thus peripheral segments show partial action potentials during the active sodium conductance increase and the rise in potential to values near E_{Na} cause the active sodium current for these segments to be small.

The implications of these simulations are most important in improving our assessment of the reversal potential of the currents in the squid giant synapse from the wide range of reported values (0 to 45 mV with respect to the extracellular ground). They indicate that the observations made in axons where the normal potassium conductance increase has been minimized by application of TEA internally are more nearly correct than for untreated axons. Furthermore they provide a correction to be applied in normal untreated axons or those with partially reduced potassium conductance changes. Many axons exhibit two to three times the conductances of the H-H equations. In these, the errors in E_s would be much larger than shown in the present simulations.

Another important observation is the marked departure of the apparent time course and amplitude of a synaptic conductance from the actual simulated values when the microelectrodes are placed outside of the synaptic area. This is of fundamental importance in the interpretation of voltage clamp records from such cells as the spinal motoneurone and *Aplysia* neurones on which there are nonsomatic synapses. The simulations described here provide a method of determining the feasibility and limitations of voltage clamp techniques on such preparations.

Another area of recent interest has been the voltage dependence of the endplate conductance at the neuromuscular junction as described by Magleby and Stevens

(1972 *a,b*). In this preparation two microelectrodes within the junction region are used to hold the membrane potential at some steady level during the synaptic transmission. A complete simulation of this technique would require a more complex cable model to include the additional effects of the tubule system as well as active properties appropriate to the muscle fiber (Adrian et al., 1970; Adrian and Peachey, 1973). Nevertheless, since the muscle membrane conductance is also a function of voltage, it seems possible that the change in the time course of the endplate conductance observed by Magleby and Stevens could be explained by changes in the degree of isopotentiality of the endplate region with changes in the holding potential. However, we have not been able to produce similar changes in the time course of the apparent synaptic conductance by changing the membrane conductance of a passive cable model for the axon. This tends to support the voltage dependence of the time course of endplate conductance, but a more exact representation as described above is needed.

We would like to thank Dr. R. Llinás for helpful comments.
We also appreciate the contributions of Mr. E. M. Harris (in maintaining the computers operational) and Mrs. D. Munday (in typing the several drafts of these papers).

We are pleased to acknowledge the support of this work by the National Institutes of Health in the form of grant NS03437.

Received for publication 17 June 1974.

REFERENCES

ADRIAN, R. H., W. K. CHANDLER, and A. L. HODGKIN. 1970. *J. Physiol. (Lond.).* **208**:607.
ADRIAN, R. H., and L. P. PEACHEY. 1973. *J. Physiol. (Lond.).* **235**:103.
ARMSTRONG, C. M., and L. BINSTOCK. 1965. *J. Gen. Physiol.* **48**:859.
COLE, K. S., and J. W. MOORE. 1960. *Biophys. J.* **1**:1.
GAGE, P. W., and J. W. MOORE. 1969. *Science (Wash. D.C.).* **166**:510.
HAGIWARA, S., and I. TASAKI. 1958. *J. Physiol. (Lond.).* **143**:114.
HODGKIN, A. L., and A. F. HUXLEY. 1952. *J. Physiol. (Lond.).* **117**:500.
MAGLEBY, K. L., and C. F. STEVENS. 1972 *a. J. Physiol. (Lond.).* **223**:151.
MAGLEBY, K. L., and C. F. STEVENS. 1972 *b. J. Physiol. (Lond.).* **223**:173.
MOORE, J. W., F. RAMÓN, and R. W. JOYNER. 1975 *a. Biophys. J.* **15**:11.
MOORE, J. W., F. RAMÓN, and R. W. JOYNER. 1975 *b. Biophys. J.* **15**:25.
MOORE, J. W., and W. ADELMAN. 1961. *J. Gen. Physiol.* **45**:77.
RAMÓN, F., N. ANDERSON, R. W. JOYNER, and J. W. MOORE. 1975. *Biophys. J.* **15**:55.
TAYLOR, R. E., J. W. MOORE, and K. S. COLE. 1960. *Biophys. J.* **1**:161.